

## Response to Referee 2:

The manuscript's abstract, introduction and conclusions are much improved based upon responses to the reviewer comments. A few important issues remain.

It's a bit of a circular argument to suggest that because they can "fit" the Freyer et al 1993 observational value for the combined LCIE and EIE of  $\sim -18$  per mil that this justifies their experimental value for the combined LCIE of  $-10$  per mil. There are several ways in which the study needs to be more quantitative in its approach to evaluating the experimental results. Currently, overall, I am unimpressed with the application to environmental data because the data under heavily controlled experimental conditions shows a great deal of variability that is not discussed. How will we ever understand this in the field, with a wide variety of complications versus the chamber experiments if we cannot even fully address the uncertainties associated with the controlled experiments?

We agree with the reviewer's point that there are still uncertainties hindering us from fully model the  $\delta^{15}\text{N}$  values of atmospheric reactive nitrogen. We would like to measure the EIE and LCIE at other temperatures in the future to advance our current understanding. However, we believe our equations that quantifying the relative importance of EIE and LCIE in the NO-NO<sub>2</sub> system should be valid although the constants could change by environment. There are a lot more work still needed to fill the knowledge gap and we are looking forward to future investigations.

Figure 1A and 1B should be dissected QUANTITATIVELY. Best fit terminology is used in the manuscript in a here qualitative manner. For Figure 1A, the actual best linear fit to the experimental results should be quantified and compared against the forced intercept line that is currently pictured. The standard error for both the slope and intercept should be calculated for the best linear fit to the data and this should be compared to assess whether the experimental results are statistically significantly different than (0,0). It appears it might be significantly different, and this should be discussed if it is (i.e., what causes the difference from (0,0)? how might this be better addressed in future experiments?).

We agree with the reviewer's point that we need to provide quantification to our fit lines in both EIE and LCIE experiments. To better demonstrate this, we added some description of the uncertainties in the figure caption and we pointed out the error bars on the figures represented the overall uncertainties of NO<sub>x</sub> concentration measurement and isotopic analysis. For the EIE line, we provided the standard error (1.2‰) and for the LCIE line we reported RMSE (1.1‰) and suggest the  $-10$ ‰ line showed the lowest RMSE when comparing to our measured data.

The response to reviewers includes discussion of the error bars in Figures 1A and 1B, but this also needs to be discussed in the main text and should be indicated in the caption what the error bars represent.

Revised as suggested.

For Figure 1B, the  $-10$  line (which is actually  $-10.5$  in the figure) is simply not the best qualitative fit to both the experimental data and the Freyer observation. Even qualitatively the

language should be changed to better address what you are trying to prove here. Better yet, I suggest quantitatively calculating what line actually fits the experimental data...you could even do this while including and excluding the Freyer datapoint. Then address how the actual best fit through the data compared with the theoretical (case-based) lines drawn in Figure 1B.

We agree with the reviewer's point that we need to provide quantification to our fit lines. In the LCIE figure, we used Rooted Mean Square Error (RMSE) to assess the fit and the -10‰ line gives the lowest RMSE of 1.1‰. We have added this part into the main text. Also, we have changed the number in the figure because with 5‰ uncertainty, the last digit has no meaning.

The lack of correction for isobaric influence needs to be directly addressed in the Methods section. This could in fact make a difference on the order of 0.5-0.8 per mil under the equations used here. While the non-zero D17O correction to d15N is probably not making a difference in the dark experiments, it could make a difference in the photochemical experiments. It is clear in the literature regarding measurement of d15N from N2O that this correction is important and there is no reason for it not at least be addressed here.

The isobaric correction when measuring atmospheric NO<sub>2</sub> is important, especially when O<sub>3</sub> participated in the reactions. In our experiment, O<sub>3</sub> played an important role during all the conversion between NO and NO<sub>2</sub> therefore we agree that all of our samples should somewhat show some isobaric error.

However, we suggest the isobaric effects should be cancelled out in our graphs when we subtract  $\delta^{15}\text{N}$  value of measured NO<sub>2</sub> with  $\delta^{15}\text{N}$  value of measured NO<sub>x</sub>. When we measure the  $\delta^{15}\text{N}$  of source NO<sub>x</sub>, we first injected O<sub>3</sub> into the chamber then injected NO and ensure 100% of NO was converted into NO<sub>2</sub>. During this process, the measured  $\delta(\text{NO}_x)$  also carried the isobaric error. Thus, when we subtract  $\delta(\text{NO}_2)$  with  $\delta(\text{NO}_x)$ , this error is likely cancelled out. This is also the reason that the five data points should be forced to have an intercept of 0 because measuring  $\delta(\text{NO}_x)$  can be seen as three individual experiments that fall on (0,0) in the figure.

The addition of Figure 1C is nice, but I would suggest adding it as Figure 1A and referring to it much earlier on (when defining EIE, LCIE and PHIFE) and then referring to it again after quantifying the values and noting that they are on the figure – the figure caption could also include the values in the figure are determined “in this work”.

Revised as suggested.

Lastly, I am confused by mention (in the response to reviewers) of Walters and Michalski assuming  $\alpha_1 - \alpha_2 = 0$ . My understanding is that the  $\alpha_1$  is assumed to be 1 such that the fractionation factor is 0;  $\alpha_2$  is theoretically determined with an  $\epsilon \sim -7$  per mil. So that would suggest that  $\alpha_1 - \alpha_2$  does not = 0. Please revisit this to be sure that this misinterpretation is not confusing the results/discussion in the manuscript.

Sorry for the confusion. We have pointed out the alpha 2 values of -7‰ in the main text and suggested a good match between the experimentally determined value (LCIE=-10±5 ‰) vs. the theoretically predicted values (alpha1=1.0026 and alpha2=0.9933).

Minor comments:

Line 65 – remove the word “be”

Revised as suggested.

Line 74 – approximations is misspelled

Revised as suggested.

Line 81 – notable should be notably

Revised as suggested.

Line 124 – ranged should be ranging

Revised as suggested.

Line 147 – remove the word “break” before NO<sub>2</sub>

Revised as suggested.

Line 419 – why mention nitrate aerosols specifically? Why would you not also compare with wet-deposited nitrate?

Revised as suggested.

Line 423-426 – need to be careful here. This addition was in response to the reviewers’ who raised concerns about this. All of the calculations done in Figure 2 are based only on changes in NO and NO<sub>2</sub> concentrations and ratios, using an alpha value that is constant. So it is important to consider that it is possible that temperature could have an impact on the interpretation of field data, and this should be investigated based upon comparisons between field collections and the laboratory experimental determinations.

Revised as suggested.

Figure 3 caption – you might add a note that points out the different y-axis for figure 3D.

Revised as suggested.

**List of changes:**

1. We changed Fig. 1 and its caption. We put the sketch as Fig. 1A and revised the captions.
2. We reported the RMSE between the LCIE line and our measured values. We suggest that the LCIE line with an LCIE factor of -10‰ gives the lowest RMSE (line 261).
3. We pointed out our study can be applied not only to nitrate aerosols but also dissolved nitrate in wet deposition (line 420).
4. We pointed out that the temperature may play an important role controlling the isotopic fractionations in the ambient environment (lines 424-428)
5. Other typo and grammar errors.

1 **Quantifying the nitrogen isotope effects during photochemical**  
2 **equilibrium between NO and NO<sub>2</sub>: implications for  $\delta^{15}\text{N}$  in**  
3 **tropospheric reactive nitrogen**

Deleted: Implications

4 Jianghanyang Li<sup>1</sup>, Xuan Zhang<sup>2</sup>, John Orlando<sup>2</sup>, Geoffrey Tyndall<sup>2</sup> and Greg Michalski<sup>1,3</sup>

5 <sup>1</sup>. Department of Earth, Atmospheric and Planetary Sciences, Purdue University, West Lafayette,  
6 IN, 47907

7 <sup>2</sup>. Atmospheric Chemistry Observations and Modeling Lab, National Center for Atmospheric  
8 Research, Boulder, CO, 80301

9 <sup>3</sup>. Department of Chemistry, Purdue University, West Lafayette, IN, 47907

10 *Correspondence to:* Jianghanyang Li (li2502@purdue.edu)

11 **Abstract.** Nitrogen isotope fractionations between nitrogen oxides (NO and NO<sub>2</sub>) play a  
12 significant role in determining the nitrogen isotopic compositions ( $\delta^{15}\text{N}$ ) of atmospheric reactive  
13 nitrogen. Both the equilibrium isotopic exchange between NO and NO<sub>2</sub> molecules and the isotope  
14 effects occurring during the NO<sub>x</sub> photochemical cycle are important, but both are not well  
15 constrained. The nighttime and daytime isotopic fractionations between NO and NO<sub>2</sub> in an  
16 atmospheric simulation chamber at atmospherically relevant NO<sub>x</sub> levels were measured. Then, the  
17 impact of NO<sub>x</sub> level and NO<sub>2</sub> photolysis rate to the combined isotopic fractionation (equilibrium  
18 isotopic exchange and photochemical cycle) between NO and NO<sub>2</sub> were calculated. It was found  
19 that the isotope effects occurring during the NO<sub>x</sub> photochemical cycle can be described using a  
20 single fractionation factor, designated the Leighton Cycle Isotope Effect (LCIE). The results  
21 showed that at room temperature, the fractionation factor of nitrogen isotopic exchange is  
22  $1.0275 \pm 0.0012$ , and the fractionation factor of LCIE (when O<sub>3</sub> solely controls the oxidation from  
23 NO to NO<sub>2</sub>) is  $0.990 \pm 0.005$ . The measured LCIE factor showed good agreement with previous  
24 field measurements, suggesting that it could be applied in ambient environment, although future  
25 work is needed to assess the isotopic fractionation factors of  $\text{NO} + \text{RO}_2/\text{HO}_2 \rightarrow \text{NO}_2$ . The results  
26 were used to model the NO-NO<sub>2</sub> isotopic fractionations under several NO<sub>x</sub> conditions. The model  
27 suggested that isotopic exchange was the dominate factor when  $\text{NO}_x > 20 \text{ nmol mol}^{-1}$ , while LCIE  
28 was more important at low NO<sub>x</sub> concentrations ( $< 1 \text{ nmol mol}^{-1}$ ) and high rates of NO<sub>2</sub> photolysis.  
29 These findings provided a useful tool to quantify the isotopic fractionations between tropospheric  
30 NO and NO<sub>2</sub>, which can be applied in future field observations and atmospheric chemistry models.  
31

Deleted: poorly

Deleted: isotope

32

36 **1. Introduction**

37 The nitrogen isotopic composition ( $\delta^{15}\text{N}$ ) of reactive nitrogen compounds in the  
38 atmosphere is an important tool in understanding the sources and chemistry of atmospheric  $\text{NO}_x$   
39 ( $\text{NO}+\text{NO}_2$ ). It has been suggested that the  $\delta^{15}\text{N}$  value of atmospheric nitrate ( $\text{HNO}_3$ , nitrate  
40 aerosols and nitrate ions in the precipitation and snow) imprints the  $\delta^{15}\text{N}$  value of  $\text{NO}_x$  sources  
41 (Elliott et al., 2009; Kendall et al., 2007) thus many studies have used the  $\delta^{15}\text{N}$  values of  
42 atmospheric nitrate to investigate  $\text{NO}_x$  sources (Chang et al., 2018; Felix et al., 2012; Felix &  
43 Elliott, 2014; Gobel et al., 2013; Hastings et al., 2004, 2009; Morin et al., 2009; Park et al., 2018;  
44 Walters et al., 2015, 2018). However, there remain questions about how isotopic fractionations  
45 that may occur during photochemical cycling of  $\text{NO}_x$  could alter the  $\delta^{15}\text{N}$  values as it partitions  
46 into  $\text{NO}_y$  ( $\text{NO}_y$  = atmospheric nitrate,  $\text{NO}_3$ ,  $\text{N}_2\text{O}_5$ ,  $\text{HONO}$ , etc., Chang et al., 2018; Freyer, 1991;  
47 Hastings et al., 2004; Jarvis et al., 2008; Michalski et al., 2005; Morin et al., 2009; Zong et al.,  
48 2017). Similarly, other complex reactive nitrogen chemistry, such as nitrate photolysis and re-  
49 deposition in ice and snow (Frey et al., 2009), may impact the  $\delta^{15}\text{N}$  of  $\text{NO}_y$  and atmospheric nitrate.  
50 The fractionation between  $\text{NO}$  and  $\text{NO}_2$  via isotope exchange has been suggested to be the  
51 dominant factor in determining the  $\delta^{15}\text{N}$  of  $\text{NO}_2$  and ultimately atmospheric nitrate (Freyer, 1991;  
52 Freyer et al., 1993; Savarino et al., 2013; Walters et al., 2016). However, isotopic fractionations  
53 occur in most, if not all,  $\text{NO}_x$  and  $\text{NO}_y$  reactions, while most of these are still unknown or, if  
54 calculated (Walters and Michalski, 2015), unverified by experiments. Since the atmospheric  
55 chemistry of  $\text{NO}_y$  varies significantly in different environments (e.g., polluted vs. pristine, night  
56 vs. day), the isotopic fractionations associated with  $\text{NO}_y$  chemistry are also likely to vary in  
57 different environments. These unknowns could potentially bias conclusions about  $\text{NO}_x$  source  
58 apportionment reached when using nitrogen isotopes. Therefore, understanding the isotopic

59 fractionations between NO and NO<sub>2</sub> during photochemical cycling could improve our  
60 understanding of the relative role of sources versus chemistry for controlling the δ<sup>15</sup>N variations  
61 of atmospheric NO<sub>2</sub> and nitrate.

62 In general, there are three types of isotopic fractionation effects associated with NO<sub>x</sub>  
63 chemistry (Fig. 1A). The first type is the equilibrium isotopic effect (EIE), i.e., isotope exchange  
64 between two compounds without forming new molecules (Urey, 1947, Bigeleisen and Mayer,  
65 1947), which for nitrogen isotopes in the NO<sub>x</sub> system is the  $^{15}\text{NO} + ^{14}\text{NO}_2 \leftrightarrow ^{14}\text{NO} + ^{15}\text{NO}_2$   
66 exchange reaction (Begun and Melton, 1956, Walters et al., 2016). The second type is the kinetic  
67 isotopic effect (KIE) associated with difference in isotopologue rate coefficients during  
68 unidirectional reactions (Bigeleisen & Wolfsberg, 1957). In the NO<sub>x</sub> system this KIE would  
69 manifest in the oxidation of NO into NO<sub>2</sub> by O<sub>3</sub>/HO<sub>2</sub>/RO<sub>2</sub>. The third type is the photochemical  
70 isotope fractionation effect (PHIFE, Miller & Yung, 2000), which for NO<sub>x</sub> is the isotopic  
71 fractionation associated with NO<sub>2</sub> photolysis. All three fractionations could impact the δ<sup>15</sup>N value  
72 of NO<sub>2</sub>, and consequently atmospheric nitrate, but the relative importance of each may vary.

73 The limited number of studies on the EIE in the NO<sub>x</sub> cycle have significant uncertainties.  
74 Discrepancies in the EIE for  $^{15}\text{NO} + ^{14}\text{NO}_2 \leftrightarrow ^{14}\text{NO} + ^{15}\text{NO}_2$  have been noted in several studies.  
75 Theoretical calculations predicted isotope fractionation factors (α) ranging from 1.035 to 1.042 at  
76 room temperature (Begun & Fletcher, 1960; Monse et al., 1969; Walters & Michalski, 2015) due  
77 to the different approximations used to calculate harmonic frequencies in each study. Likewise,  
78 two separate experiments measured different room temperature fractionation factors of  
79  $1.028 \pm 0.002$  (Begun & Melton, 1956) and  $1.0356 \pm 0.0015$  (Walters et al., 2016). A concern in both  
80 experiments is that they were conducted in small chambers with high NO<sub>x</sub> concentrations  
81 (hundreds of μmol mol<sup>-1</sup>), significantly higher than typical ambient atmospheric NO<sub>x</sub> levels

Deleted: isotope

Deleted: be

Deleted: approximations

85 (usually less than  $0.1 \mu\text{mol mol}^{-1}$ ). Whether the isotopic fractionation factors determined by these  
86 experiments are applicable in the ambient environment is uncertain because of possible wall effects  
87 and formation of higher oxides, notably  $\text{N}_2\text{O}_4$  and  $\text{N}_2\text{O}_3$  at these high  $\text{NO}_x$  concentrations.

Deleted: notable

88 Even less research has examined the KIE and PHIFE occurring during  $\text{NO}_x$  cycling. The  
89 KIE of  $\text{NO} + \text{O}_3$  has been theoretically calculated (Walters and Michalski, 2016) but has not been  
90 experimentally verified. The  $\text{NO}_2$  PHIFE has not been experimentally determined or theoretically  
91 calculated. As a result, field observation studies often overlook the effects of PHIFE and KIE.  
92 Freyer et al. (1993) measured  $\text{NO}_x$  concentrations and the  $\delta^{15}\text{N}$  values of  $\text{NO}_2$  over a 1-year period  
93 at Jülich, Germany and inferred a combined  $\text{NO}_x$  isotope fractionation factor (EIE+KIE+PHIFE)  
94 of  $1.018 \pm 0.001$ . Freyer et al. (1993) suggested that the  $\text{NO}_x$  photochemical cycle (KIE and PHIFE)  
95 tends to diminish the equilibrium isotopic fractionation (EIE) between  $\text{NO}$  and  $\text{NO}_2$ . Even if this  
96 approach were valid, applying this single fractionation factor elsewhere, where  $\text{NO}_x$ ,  $\text{O}_3$   
97 concentrations and actinic fluxes are different, would be tenuous given that these factors may  
98 influence the relative importance of EIE, KIE and PHIFE (Hastings et al., 2004; Walters et al.,  
99 2016). Therefore, to quantify the overall isotopic fractionations between  $\text{NO}$  and  $\text{NO}_2$  at various  
100 tropospheric conditions, it is crucial to know 1) isotopic fractionation factors of EIE, KIE and  
101 PHIFE individually and 2) the relative importance of each factor under various conditions.

102 In this work, we aim to quantify the nitrogen isotope fractionation factors between  $\text{NO}$  and  
103  $\text{NO}_2$  at photochemical equilibrium. First, we measure the N isotope fractionations between  $\text{NO}$   
104 and  $\text{NO}_2$  in an atmospheric simulation chamber at atmospherically relevant  $\text{NO}_x$  levels. Then, we  
105 provide mathematical solutions to assess the impact of  $\text{NO}_x$  level and  $\text{NO}_2$  photolysis rate ( $j(\text{NO}_2)$ )  
106 to the relative importance of EIE, KIE and PHIFE. Subsequently we use the solutions and chamber  
107 measurements to calculate the isotopic fractionation factors of EIE, KIE and PHIFE. Lastly, using

Deleted: d



110 the calculated fractionation factors and the equations, we model the NO-NO<sub>2</sub> isotopic  
111 fractionations at several sites to illustrate the behavior of δ<sup>15</sup>N values of NO<sub>x</sub> in the ambient  
112 environment.

113

## 114 2. Methods

115 The experiments were conducted using a 10 m<sup>3</sup> Atmospheric Simulation Chamber at the  
116 National Center for Atmospheric Research (see descriptions in supplementary material and Zhang  
117 et al. (2018)). A set of mass flow controllers was used to inject NO and O<sub>3</sub> into the chamber. NO  
118 was injected at 1 L min<sup>-1</sup> from an in-house NO/N<sub>2</sub> cylinder (133.16 μmol mol<sup>-1</sup> NO in ultra-pure  
119 N<sub>2</sub>), and O<sub>3</sub> was generated by flowing 5 L min<sup>-1</sup> zero-air through a flow tube equipped with a UV  
120 Pen-Ray lamp (UVP LLC., CA) into the chamber. NO and NO<sub>2</sub> concentrations were monitored in  
121 real time by chemiluminescence with a detection limit of 0.5 ppb (model CLD 88Y, Eco Physics,  
122 MI) as were O<sub>3</sub> concentrations using an UV absorption spectroscopy with a detection limit of 0.5  
123 ppb (model 49, Thermo Scientific, CO). In each experiment, the actual amounts of NO and O<sub>3</sub>  
124 injected were calculated using measured NO<sub>x</sub> and O<sub>3</sub> concentrations after steady state was reached  
125 (usually within 1 h). The wall loss rate of NO<sub>2</sub> was tested by monitoring O<sub>3</sub> (29 nmol mol<sup>-1</sup>) and  
126 NO<sub>x</sub> (62 nmol mol<sup>-1</sup>) over a 4-hour period. After the NO and NO<sub>2</sub> concentrations reached steady  
127 state, no decrease in NO<sub>2</sub> concentrations was observed showing that chamber wall loss was  
128 negligible.

129 Two sets of experiments were conducted to separately investigate the EIE, KIE and PHIFE.  
130 The first set of experiments was conducted in the dark. In each of these dark experiments, a range  
131 of NO and O<sub>3</sub> ([O<sub>3</sub>] < [NO]) was injected into the chamber to produce NO-NO<sub>2</sub> mixtures with  
132 [NO]/[NO<sub>2</sub>] ratios ranging from 0.43 to 1.17. The N isotopes of these mixtures were used to

Deleted: ed

Deleted: ranged

135 investigate the EIE between NO and NO<sub>2</sub>. The second set of experiments was conducted under  
136 irradiation of UV lights (300-500 nm, see supplementary material for irradiation spectrum). Under  
137 such conditions, NO, NO<sub>2</sub> and O<sub>3</sub> reached photochemical steady state, which combined the  
138 isotopic effects of EIE, KIE and PHIFE. In addition, three experiments were conducted to measure  
139 the δ<sup>15</sup>N value of the tank NO. In each of these experiments, a certain amount of O<sub>3</sub> was first  
140 injected into the chamber, then approximately the same amount of NO was injected into the  
141 chamber to ensure 100% of the NO<sub>x</sub> was in the form of NO<sub>2</sub> with little O<sub>3</sub> (<3 nmol mol<sup>-1</sup>)  
142 remaining in the chamber, such that the O<sub>3</sub>+NO<sub>2</sub> reaction was negligible. The NO<sub>2</sub> in the chamber  
143 was then collected and its δ<sup>15</sup>N value measured, which equates to the δ<sup>15</sup>N value of the tank NO.

144 In all experiments, the concentrations of NO, NO<sub>2</sub> and O<sub>3</sub> were allowed to reach steady  
145 state, and the product NO<sub>2</sub> was collected from the chamber using a honeycomb denuder tube. The  
146 glass denuder tubes (Chemcomb 3500, Thermo Fisher Scientific) were coated with a solution of  
147 10% KOH and 25% guaiacol in methanol and then dried by flowing N<sub>2</sub> gas through the denuder  
148 tube for 15 seconds (Williams and Grosjean, 1990, Walters et al., 2016). The NO<sub>2</sub> reacted with  
149 guaiacol coating and was converted into NO<sub>2</sub><sup>-</sup> that was retained on the denuder tube wall (Williams  
150 and Grosjean, 1990). NO was inert to the denuder tube coating: a control experiment sampled pure  
151 NO using the denuder tubes, which did not show any measurable NO<sub>2</sub><sup>-</sup>. The NO<sub>2</sub> collection  
152 efficiency of a single honeycomb denuder tube was tested in another control experiment: air  
153 containing 66 nmol mol<sup>-1</sup> of NO<sub>2</sub> was drawn out of the chamber through a denuder tube, and the  
154 NO<sub>2</sub> concentration at the exit of the tube holder was measured and found to be below the detection  
155 limit (<1 nmol mol<sup>-1</sup>), suggesting the collection efficiency was nearly 100% when [NO<sub>2</sub>] <66 nmol  
156 mol<sup>-1</sup>. Furthermore, when the denuder system consisted of two denuder tubes in series and NO<sub>2</sub><sup>-</sup> in  
157 the second denuder was below the detection limit indicating trivial NO<sub>2</sub> breakthrough. The NO<sub>2</sub><sup>-</sup>

Deleted: reacts

Deleted: is

Deleted: is

Deleted: is

Deleted: break

163 was leached from each denuder tube by rinsing thoroughly with 10 ml deionized water into a clean  
164 polypropylene container and stored frozen until isotopic analysis. Isotopic analysis was conducted  
165 at Purdue Stable Isotope Laboratory. For each sample, approximately 50 nmol of the  $\text{NO}_2^-$  extract  
166 was mixed with 2 M sodium azide solution in acetic acid buffer in an air-tight glass vial, then  
167 shaken overnight to completely reduce all the  $\text{NO}_2^-$  to  $\text{N}_2\text{O}_{(\text{g})}$  (Casciotti & McIlvin, 2007; McIlvin  
168 & Altabet, 2005). The product  $\text{N}_2\text{O}$  was directed into a Thermo GasBench equipped with cryo-  
169 trap, then the  $\delta^{15}\text{N}$  of the  $\text{N}_2\text{O}$  was measured using a Delta-V Isotope Ratios Mass Spectrometer.  
170 Six coated denuders tubes that did not get exposed to  $\text{NO}_2$  were also analyzed using the same  
171 chemical procedure, which did not show any measurable signal on the IRMS, suggesting the blank  
172 from both sampling process and the chemical conversion process was negligible. The overall  
173 analytical uncertainty for  $\delta^{15}\text{N}$  analysis was  $\pm 0.5 \text{ ‰}$  ( $1\sigma$ ) based on replicate analysis of in house  
174  $\text{NO}_2^-$  standards.

175

### 176 3. Results and Discussions

#### 177 3.1. Equilibrium Isotopic Fractionation between NO and $\text{NO}_2$

178 The equilibrium isotope fractionation factor,  $\alpha(\text{NO}_2\text{-NO})$ , is the  $^{15}\text{N}$  enrichment in  $\text{NO}_2$   
179 relative to  $\text{NO}$ , and is expressed as the ratio of rate constants  $k_2/k_1$  of two reactions:



182 where  $k_1$  is the rate constant of the isotopic exchange, which was previously determined to be  
183  $8.14 \times 10^{-14} \text{ cm}^3 \text{ s}^{-1}$  (Sharma et al., 1970). The reaction time required for  $\text{NO-NO}_2$  to reach isotopic  
184 equilibrium was estimated using the exchange rate constants in a simple kinetics box model  
185 (BOXMOX, Knote et al., 2015). The model predicts that at typical  $\text{NO}_x$  concentrations used during

186 the chamber experiments (7.7-62.4 nmol mol<sup>-1</sup>), isotopic equilibrium would be reached within 15  
 187 minutes (see supplementary [material](#)). Since the sample collection usually started 1 hour after NO<sub>x</sub>  
 188 was well mixed in the chamber, there was sufficient time to reach full isotope equilibrium. The  
 189 isotope equilibrium fractionation factor is then calculated to be:

$$190 \quad \alpha(\text{NO}_2 - \text{NO}) = \frac{[^{15}\text{NO}_2] \times [^{14}\text{NO}]}{[^{14}\text{NO}_2] \times [^{15}\text{NO}]} = \frac{R(\text{NO}_2)}{R(\text{NO})} \quad \text{Eq. (1)}$$

191 where R(NO, NO<sub>2</sub>) are the <sup>15</sup>N/<sup>14</sup>N ratios of NO and NO<sub>2</sub>. By definition, the  
 192 δ<sup>15</sup>N(NO)=(R(NO)/R(reference) -1)×1000‰ and δ<sup>15</sup>N(NO<sub>2</sub>)=(R(NO<sub>2</sub>)/R(reference)-1) × 1000 ‰,  
 193 but hereafter, the δ<sup>15</sup>N values of NO, NO<sub>2</sub> and NO<sub>x</sub> will be referred as δ(NO), δ(NO<sub>2</sub>) and δ(NO<sub>x</sub>),  
 194 respectively. Eq. (1) leads to:

$$195 \quad \delta(\text{NO}_2) - \delta(\text{NO}) = (\alpha(\text{NO}_2 - \text{NO}) - 1) \times 1000 \text{‰} \times (1 + \delta(\text{NO})) \\
 196 \quad \quad \quad = \varepsilon(\text{NO}_2 - \text{NO}) \times (1 + \delta(\text{NO})) \quad \text{Eq. (2)}$$

197 where ε(NO<sub>2</sub>-NO) is the isotope enrichment factor (ε(NO<sub>2</sub>-NO)=(α(NO<sub>2</sub>-NO)-1)×1000‰, Hoefs,  
 198 2009). Using Eq. (2) and applying NO<sub>x</sub> isotopic mass balance (δ(NO<sub>x</sub>)=f(NO<sub>2</sub>)×δ(NO<sub>2</sub>)+(1-  
 199 f(NO<sub>2</sub>))×δ(NO), f(NO<sub>2</sub>)=[NO<sub>2</sub>]/([NO]+[NO<sub>2</sub>])) yields:

$$200 \quad \delta(\text{NO}_2) - \delta(\text{NO}_x) = \varepsilon(\text{NO}_2 - \text{NO}) \times (1 + \varepsilon(\text{NO}_2 - \text{NO})) \times (1 + \delta(\text{NO}_2)) \times (1 - f(\text{NO}_2)) \quad \text{Eq. (3)}$$

201 Here, δ(NO<sub>x</sub>) equals to the δ<sup>15</sup>N value of the cylinder NO and f(NO<sub>2</sub>) is the molar fraction of NO<sub>2</sub>  
 202 with respect to total NO<sub>x</sub>. Three experiments (see descriptions in method section) that measured  
 203 δ(NO<sub>x</sub>) showed consistent δ(NO<sub>x</sub>) values of -58.7±0.8 ‰ (n = 3), indicating δ(NO<sub>x</sub>) remained  
 204 unchanged throughout the experiments (as expected for isotope mass balance). Thus, the δ(NO<sub>x</sub>)  
 205 can be treated as a constant in Eq. (3), and the linear regression of (δ(NO<sub>2</sub>)-δ(NO<sub>x</sub>))/(1+δ(NO<sub>2</sub>))  
 206 versus 1-f(NO<sub>2</sub>) should have an intercept of 0 and a slope of ε(NO<sub>2</sub>-NO)/(1+ε(NO<sub>2</sub>-NO)).

Deleted: information

Deleted:

Deleted: ,

Deleted: (

Deleted:

Deleted: slope of a

Deleted: yields

214 The plot of  $(\delta(\text{NO}_2)-\delta(\text{NO}_x))/(1+\delta(\text{NO}_2))$  as a function of  $1-f(\text{NO}_2)$  values from five  
215 experiments yields an  $\epsilon(\text{NO}_2\text{-NO})$  value of  $27.5\pm 1.2$  ‰ at room temperature (Fig. 1B). This  
216 fractionation factor is comparable to previously measured values but with some differences. Our  
217 result agrees well with the  $\alpha(\text{NO}_2\text{-NO})$  value of  $1.028\pm 0.002$  obtained by Begun and Melton (1956)  
218 at room temperature. However, Walters et al., (2016) determined the  $\alpha(\text{NO}_2\text{-NO})$  values of NO-  
219 NO<sub>2</sub> exchange in a 1-liter reaction vessel, which showed a slightly higher  $\alpha(\text{NO}_2\text{-NO})$  value of  
220 1.035. This discrepancy might originate from rapid heterogeneous reactions on the wall of the  
221 reaction vessel at high NO<sub>x</sub> concentrations and the small chamber size used by Walters et al. (2016).  
222 They used a reaction vessel made of Pyrex, which is known to absorb water (Do Remus et al.,  
223 1983; Takei et al., 1997) that can react with NO<sub>2</sub> forming HONO, HNO<sub>3</sub> and other N compounds.  
224 Additionally, previous studies have suggested that Pyrex walls enhance the formation rate of N<sub>2</sub>O<sub>4</sub>  
225 by over an order of magnitude (Barney & Finlayson-Pitts, 2000; Saliba et al., 2001), which at  
226 isotopic equilibrium is enriched in <sup>15</sup>N compared to NO and NO<sub>2</sub> (Walters & Michalski, 2015).  
227 Therefore, their measured  $\alpha(\text{NO}_2\text{-NO})$  might be slightly higher than the actual  $\alpha(\text{NO}_2\text{-NO})$  value.  
228 In this work, the 10 m<sup>3</sup> chamber has a much smaller surface to volume ratio relative to Walters et  
229 al. (2016) which minimizes wall effects, and the walls were made of Teflon that minimize NO<sub>2</sub>  
230 surface reactivity, which was evidenced by the NO<sub>2</sub> wall loss control experiment. Furthermore,  
231 the low NO<sub>x</sub> mixing ratios in our experiments minimized N<sub>2</sub>O<sub>4</sub> and N<sub>2</sub>O<sub>3</sub> formation. At NO and  
232 NO<sub>2</sub> concentrations of 50 nmol mol<sup>-1</sup> the steady state concentrations of N<sub>2</sub>O<sub>4</sub> and N<sub>2</sub>O<sub>3</sub> were  
233 calculated to be 0.014 and 0.001 pmol mol<sup>-1</sup>, respectively (Atkinson et al., 2004). Therefore, we  
234 suggest our measured  $\alpha(\text{NO}_2\text{-NO})$  value ( $1.0275\pm 0.0012$ ) may better reflect the room temperature  
235 (298 K) NO-NO<sub>2</sub> EIE in the ambient environment.

Deleted: yielded

Deleted:

238 Unfortunately, the chamber temperature could not be controlled so we were not able to  
 239 investigate the temperature dependence of the EIE. Hence, we speculate that the  $\alpha(\text{NO}_2\text{-NO})$   
 240 follows a similar temperature dependence pattern calculated in Walters et al. (2016). Walters et al.  
 241 (2016) suggested that, the  $\varepsilon(\text{NO}_2\text{-NO})$  value would be 4.7 ‰ higher at 273 K and 2.0 ‰ lower at  
 242 310 K, relative to room temperature (298 K). Using this pattern and our experimentally determined  
 243 data, we suggest the  $\alpha(\text{NO}_2\text{-NO})$  values at 273 K, 298 K and 310 K are  $32.2\pm 1.2$  ‰,  $27.5\pm 1.2$  ‰  
 244 and  $25.5\pm 1.2$  ‰, respectively. This 6.7‰ variation at least partially contribute to the daily and  
 245 seasonal variations of  $\delta^{15}\text{N}$  values of  $\text{NO}_2$  and nitrate in some areas (e.g., polar regions with strong  
 246 seasonal temperature variation). Thus, future investigations should be conducted to verify the EIE  
 247 temperature dependence.

248

### 249 3.2. Kinetic isotopic fractionation of Leighton Cycle

250 The photochemical reactions of  $\text{NO}_x$  will compete with the isotope exchange fractionations  
 251 between NO and  $\text{NO}_2$ . The NO- $\text{NO}_2$  photochemical cycle in the chamber was controlled by the  
 252 Leighton cycle:  $\text{NO}_2$  photolysis and the  $\text{NO} + \text{O}_3$  reaction. This is because there were no VOCs in  
 253 the chamber so no  $\text{RO}_2$  was produced, which excludes the  $\text{NO} + \text{RO}_2$  reaction. Likewise, the low  
 254 water vapor content ( $\text{RH} < 10\%$ ) and the minor flux of photons  $< 310$  nm results in minimal OH  
 255 production and hence little  $\text{HO}_2$  formation and subsequently trivial amount of  $\text{NO}_2$  would be  
 256 formed by  $\text{NO} + \text{HO}_2$ . Applying these limiting assumptions, the EIE between NO and  $\text{NO}_2$  (R1-  
 257 R2) were only competing with the KIE (R3-R4) and the PHIFE in R5-R6:



261  $^{15}\text{NO} + \text{O}_3 \rightarrow ^{15}\text{NO}_2 + \text{O}_2$  R6, rate constant =  $k_5 \times \alpha_2$

262 In which  $j(\text{NO}_2)$  is the  $\text{NO}_2$  photolysis rate ( $1.4 \times 10^{-3} \text{ s}^{-1}$  in these experiments),  $k_5$  is the rate constant  
 263 for the  $\text{NO} + \text{O}_3$  reaction ( $1.73 \times 10^{-14} \text{ cm}^3 \text{ s}^{-1}$ , Atkinson et al., 2004), and  $\alpha_{1,2}$  are isotopic  
 264 fractionation factors for the two reactions. Previous studies (Freyer et al., 1993; Walters et al.,  
 265 2016) have attempted to assess the competition between EIE (R1-R2), KIE and PHIFE (R3-R6),  
 266 but none of them quantified the relative importance of the two processes, nor were  $\alpha_1$  or  $\alpha_2$  values  
 267 experimentally determined. Here we provide the mathematical solution of EIE, KIE and PHIFE to  
 268 illustrate how R1-R6 affect the isotopic fractionations between  $\text{NO}$  and  $\text{NO}_2$ .

269 First, the  $\text{NO}_2$  lifetime with respect to isotopic exchange with  $\text{NO}$  ( $\tau_{\text{exchange}}$ ) and photolysis  
 270 ( $\tau_{\text{photo}}$ ) was determined:

271 
$$\tau_{\text{exchange}} = \frac{1}{k_1 \times [\text{NO}]}$$
 Eq. (4)

272 
$$\tau_{\text{photo}} = \frac{1}{j(\text{NO}_2)}$$
 Eq. (5)

273 We then define an A factor:

274 
$$A = \begin{cases} \frac{\tau_{\text{exchange}}}{\tau_{\text{photo}}} & \text{when } j(\text{NO}_2) \neq 0 \\ 0 & \text{when } j(\text{NO}_2) = 0 \end{cases}$$
 Eq. (6)

275 Using R1-R6 and Eq. (1)-(6), we solved steady-state  $\delta(\text{NO}_2)$  and  $\delta(\text{NO})$  values (see calculations  
 276 in supplementary material). Our calculations show that the  $\delta(\text{NO}_2) - \delta(\text{NO})$  and  $\delta(\text{NO}_2) - \delta(\text{NO}_x)$   
 277 values at steady state can be expressed as functions of  $\alpha_1$ ,  $\alpha_2$ ,  $\alpha(\text{NO}_2 - \text{NO})$  and A:

278 
$$\delta(\text{NO}_2) - \delta(\text{NO}) (\text{‰}) = \frac{(\alpha_2 - \alpha_1) \times A + (\alpha(\text{NO}_2 - \text{NO}) - 1)}{A + 1} \times 1000 \text{ ‰}$$
 Eq. (7)

279 
$$\delta(\text{NO}_2) - \delta(\text{NO}_x) (\text{‰}) = \frac{(\alpha_2 - \alpha_1) \times A + (\alpha(\text{NO}_2 - \text{NO}) - 1)}{A + 1} \times (1 - f(\text{NO}_2)) \times 1000 \text{ ‰}$$
 Eq. (8)

280 Equation (7) shows the isotopic fractionation between  $\text{NO}$  and  $\text{NO}_2$  ( $\delta(\text{NO}_2) - \delta(\text{NO})$ ) is largely  
 281 determined by A, the EIE factor ( $\alpha(\text{NO}_2 - \text{NO}) - 1$ ) and the  $(\alpha_2 - \alpha_1)$  factor. This  $(\alpha_2 - \alpha_1)$  represents a

282 combination of KIE and PHIFE, suggesting they act together as one factor; therefore, we name the  
283  $(\alpha_2-\alpha_1)$  factor Leighton Cycle Isotopic Effect, i.e., LCIE. Using measured  $\delta(\text{NO}_2)$ - $\delta(\text{NO})$  values,  
284 A values, and the previously determined EIE factor, we calculated that the best fit for the LCIE  
285 factor was  $-10\pm 5\text{‰}$  (showing the lowest Rooted Mean Square Error, RMSE, of 1.1%, Fig. 1C).  
286 The uncertainties in the LCIE factor are relatively higher than that of the EIE factor, mainly  
287 because of the accumulated analytical uncertainties at low  $\text{NO}_x$  and  $\text{O}_3$  concentrations, and low A  
288 values (0.10-0.28) due to the relatively low  $j(\text{NO}_2)$  value ( $1.4\times 10^{-3}\text{ s}^{-1}$ ) under the chamber  
289 irradiation conditions.

290 This LCIE factor determined in our experiments is in good agreement with theoretical  
291 calculations. Walters and Michalski (2016) previously used an *ab initio* approach to determine an  
292  $\alpha_2$  value of 0.9933 at room temperature, 0.9943 at 237 K and 0.9929 at 310 K. The variation of  $\alpha_2$   
293 values from 273 K to 310 K is only  $\pm 0.7\text{‰}$ , significantly smaller than our experimental uncertainty.  
294 The  $\alpha_1$  value was calculated using a ZPE shift model (Miller & Yung, 2000) to calculate the  
295 isotopic fractionation of  $\text{NO}_2$  by photolysis. Briefly, this model assumes both isotopologues have  
296 the same quantum yield function and the PHIFE was only caused by the differences in the  $^{15}\text{NO}_2$   
297 and  $^{14}\text{NO}_2$  absorption cross-section as a function of wavelength, thus  $\alpha_1$  values do not vary by  
298 temperature. The  $^{15}\text{NO}_2$  absorption cross-section was calculated by shifting the  $^{14}\text{NO}_2$  absorption  
299 cross-section by the  $^{15}\text{NO}_2$  zero-point energy (Michalski et al., 2004). When the ZPE shift model  
300 was used with the irradiation spectrum of the chamber lights, the resulting  $\alpha_1$  value was 1.0023.  
301 Therefore, the theoretically predicted  $\alpha_2-\alpha_1$  value should be -0.0090, i.e.,  $-9.0\pm 0.7\text{‰}$  when  
302 temperature ranges from 273 K to 310 K. This result shows excellent agreement with our  
303 experimentally determined room temperature  $\alpha_2-\alpha_1$  value of  $-10\pm 5\text{‰}$ .

Deleted: r = 0.52

Deleted: 1B



306 This model was then used to evaluate the variations of  $\alpha_1$  value to different lighting  
307 conditions. The TUV model (TUV5.3.2, Madronich & Flocke, 1999) was used to calculate the  
308 solar wavelength spectrum at three different conditions: early morning/late afternoon (solar zenith  
309 angle=85 degree), mid-morning/afternoon (solar zenith angle=45 degree), noon (solar zenith  
310 angle=0 degree). These spectrums were used in the ZPE shift model to calculate the  $\alpha_1$  values,  
311 which are 1.0025, 1.0028, and 1.0029 at solar zenith angles of 85, 45 and 0 degree, respectively.  
312 These values, along with the predicted  $\alpha_1$  value in the chamber, showed a total span of 0.6‰  
313 (1.0026  $\pm$  0.0003), which is again significantly smaller than our measured uncertainty. Therefore,  
314 we suggest that our experimentally determined LCIE factor (-10 $\pm$ 5 ‰) can be used in most  
315 tropospheric solar irradiation spectrums.

316 The equations can also be applied in tropospheric environments to calculate the combined  
317 isotopic fractionations of EIE and LCIE for NO and NO<sub>2</sub>. First, the NO<sub>2</sub> sink reactions (mainly  
318 NO<sub>2</sub>+OH in the daytime) are at least 2-3 orders of magnitude slower than the Leighton cycle and  
319 the NO-NO<sub>2</sub> isotope exchange reactions (Walters et al., 2016), therefore their effects on the  $\delta$ (NO<sub>2</sub>)  
320 should be minor. Second, although the conversion of NO into NO<sub>2</sub> in the ambient environment is  
321 also controlled by NO + RO<sub>2</sub> and HO<sub>2</sub> in addition to NO+O<sub>3</sub> (e.g., King et al., 2001), Eq. (7) still  
322 showed good agreement with field observations in previous studies. Freyer et al. (1993)  
323 determined the annual average daytime  $\delta$ (NO<sub>2</sub>)- $\delta$ (NO) at Julich, Germany along with average  
324 daytime NO concentration (9 nmol mol<sup>-1</sup>, similar to our experimental conditions) to be  
325 +18.03 $\pm$ 0.98 ‰. Using Eq. (7), assuming the daytime average  $j$ (NO<sub>2</sub>) value throughout the year  
326 was 5.0 $\pm$ 1.0 $\times$ 10<sup>-3</sup>, and a calculated A value from measured NO<sub>x</sub> concentration ranged from 0.22-  
327 0.33, the average NO-NO<sub>2</sub> fractionation factor was calculated to be +18.8 $\pm$ 1.4 ‰ (Fig. 1C), in  
328 excellent agreement with the measurements in the present study. This agreement suggests the

Deleted: 1B

330 NO+RO<sub>2</sub>/HO<sub>2</sub> reactions might have similar fractionation factors as NO+O<sub>3</sub>. Therefore, we suggest  
331 Eq. (7) and (8) can be used to estimate the isotopic fractionations between NO and NO<sub>2</sub> in the  
332 troposphere.

Deleted: (Fig. 1C)

333

### 334 3.3 Calculating nitrogen isotopic fractionations of NO-NO<sub>2</sub>

335 First, Eq. (7) was used to calculate the  $\Delta(\text{NO}_2\text{-NO}) = \delta(\text{NO}_2) - \delta(\text{NO})$  at a wide range of  
336 NO<sub>x</sub> concentrations,  $f(\text{NO}_2)$  and  $j(\text{NO}_2)$  values (Fig. 2A-D).  $j(\text{NO}_2)$  values of 0 s<sup>-1</sup> (Fig. 2A),  
337  $1.4 \times 10^{-3}$  s<sup>-1</sup> (Fig. 2B),  $5 \times 10^{-3}$  s<sup>-1</sup> (Fig. 2C) and  $1 \times 10^{-2}$  s<sup>-1</sup> (Fig. 2D) were selected to represent  
338 nighttime, dawn (as well as the laboratory conditions of our experiments), daytime average and  
339 noon, respectively. Each panel represented a fixed  $j(\text{NO}_2)$  value, and the  $\Delta(\text{NO}_2\text{-NO})$  values were  
340 calculated as a function of the A value, which was derived from NO<sub>x</sub> concentration and  $f(\text{NO}_2)$ .  
341 The A values have a large span, from 0 to 500, depending on the  $j(\text{NO}_2)$  value and the NO  
342 concentration. When A=0 ( $j(\text{NO}_2)=0$ ) and  $f(\text{NO}_2)<1$  (meaning NO-NO<sub>2</sub> coexist and [O<sub>3</sub>]=0), Eq.  
343 (7) and (8) become Eq. (2) and (3), showing the EIE was the sole factor, the  $\Delta(\text{NO}_2\text{-NO})$  values  
344 were solely controlled by EIE which has a constant value of +27.5 ‰ at 298K (Fig. 2A). When  
345  $j(\text{NO}_2)>0$ , the calculated  $\Delta(\text{NO}_2\text{-NO})$  values showed a wide range from -10.0 ‰ (controlled by  
346 LCIE factor:  $\alpha_2 - \alpha_1 = -10$  ‰) to +27.5 ‰ (controlled by EIE factor:  $\alpha(\text{NO}_2\text{-NO}) - 1 = +27.5$  ‰). Fig.  
347 2B-D display the transition from a LCIE-dominated regime to an EIE-dominated regime. The  
348 LCIE-dominated regime is characterized by low [NO<sub>x</sub>] (<50 pmol mol<sup>-1</sup>), representing remote  
349 ocean areas and polar regions (Beine et al., 2002; Custard et al., 2015). At this range the A value  
350 can be greater than 200, thus Eq. (7) can be simplified as:  $\Delta(\text{NO}_2\text{-NO}) = (\alpha_2 - \alpha_1) \times 1000$  ‰,  
351 suggesting the LCIE almost exclusively controls the NO-NO<sub>2</sub> isotopic fractionation. The  $\Delta(\text{NO}_2\text{-}$   
352 NO) values of these regions are predicted to be <0 ‰ during most time of the day and < -5 ‰ at

354 noon. On the other hand, the EIE-dominated regime was characterized by high  $[\text{NO}_x]$  ( $>20 \text{ nmol}$   
355  $\text{mol}^{-1}$ ) and low  $f(\text{NO}_2)$  ( $< 0.6$ ), representative of regions with intensive NO emissions, e.g., near  
356 roadside or stack plumes (Clapp & Jenkin, 2001; Kimbrough et al., 2017). In this case, the  $\tau_{\text{exchange}}$   
357 are relatively short (10-50 s) compared to the  $\tau_{\text{photo}}$  (approximately 100 s at noon and 1000 s at  
358 dawn), therefore the A values are small (0.01-0.5). The EIE factor in this regime thus is much more  
359 important than the LCIE factor, resulting in high  $\Delta(\text{NO}_2\text{-NO})$  values ( $>20 \text{ ‰}$ ). Between the two  
360 regimes, both EIE and LCIE are competitive and therefore it is necessary to use Eq. (7) to quantify  
361 the  $\Delta(\text{NO}_2\text{-NO})$  values.

362 Fig. 2 also implies that changes in the  $j(\text{NO}_2)$  value can cause the diurnal variations in  
363  $\Delta(\text{NO}_2\text{-NO})$  values. Changing  $j(\text{NO}_2)$  would affect the value of A and consequently the NO-NO<sub>2</sub>  
364 isotopic fractionations in two ways: 1) changes in  $j(\text{NO}_2)$  value would change the photolysis  
365 intensity, therefore the  $\tau_{\text{photo}}$  value; 2) in addition, changes in  $j(\text{NO}_2)$  value would also alter the  
366 steady state NO concentration, therefore changing the  $\tau_{\text{exchange}}$  (Fig. 2C). The combined effect of  
367 these two factors on the A value varies along with the atmospheric conditions, and thus needs to  
368 be carefully calculated using NO<sub>x</sub> concentration data and atmospheric chemistry models.

369 We then calculated the differences of  $\delta^{15}\text{N}$  values between NO<sub>2</sub> and total NO<sub>x</sub>, e.g.  $\Delta(\text{NO}_2\text{-}$   
370  $\text{NO}_x) = \delta(\text{NO}_2) - \delta(\text{NO}_x)$  in Fig. 2E-H. Since  $\Delta(\text{NO}_2\text{-NO}_x)$  are connected through the observed  $\delta^{15}\text{N}$   
371 of NO<sub>2</sub> (or nitrate) to the  $\delta^{15}\text{N}$  of NO<sub>x</sub> sources, this term might be useful in field studies (e.g.,  
372 Chang et al., 2018; Zong et al., 2017). The calculated  $\Delta(\text{NO}_2\text{-NO}_x)$  values (Fig. 2E-H) also showed  
373 a LCIE-dominated regime at low  $[\text{NO}_x]$  and an EIE-dominated regime at high  $[\text{NO}_x]$ . The  $\Delta(\text{NO}_2\text{-}$   
374  $\text{NO}_x)$  values were dampened by the  $1-f(\text{NO}_2)$  factor comparing to  $\Delta(\text{NO}_2\text{-NO})$ , as shown in Eq.  
375 (3) and (8):  $\Delta(\text{NO}_2\text{-NO}_x) = \Delta(\text{NO}_2\text{-NO}) \times (1-f(\text{NO}_2))$ . At high  $f(\text{NO}_2)$  values ( $>0.8$ ), the differences  
376 between  $\delta(\text{NO}_2)$  and  $\delta(\text{NO}_x)$  were less than 5 ‰, thus the measured  $\delta(\text{NO}_2)$  values were similar to

377  $\delta(\text{NO}_x)$ , although the isotopic fractionation between NO and  $\text{NO}_2$  could be noteworthy. Some  
378 ambient environments with significant NO emissions or high  $\text{NO}_2$  photolysis rates usually have  
379  $f(\text{NO}_2)$  values between 0.4-0.8 (Mazzeo et al., 2005; Vicars et al., 2013). In this scenario, the  
380  $\Delta(\text{NO}_2\text{-NO}_x)$  values in Fig. 2F-H showed wide ranges of -4.8 ‰ to +15.6 ‰, -6.0 ‰ to +15.0 ‰,  
381 and -6.3 ‰ to +14.2 ‰ at  $j(\text{NO}_2)=1.4\times 10^{-3} \text{ s}^{-1}$ ,  $5\times 10^{-3} \text{ s}^{-1}$ ,  $1\times 10^{-2} \text{ s}^{-1}$ , respectively. These significant  
382 differences again highlighted the importance of both LCIE and EIE (Eq. (7) and (8)) in calculating  
383 the  $\Delta(\text{NO}_2\text{-NO}_x)$ . In the following discussion, we assume 1) the  $\alpha_1$  value remain constant (see  
384 discussion above), 2) the  $\text{NO}+\text{RO}_2/\text{HO}_2$  reactions have the same fractionation factors ( $\alpha_2$ ) as  
385  $\text{NO}+\text{O}_3$ , and 3) both EIE and LCIE do not display significant temperature dependence, then use  
386 Equations (7) and (8) and this laboratory determined LCIE factor (-10 ‰) to calculate the nitrogen  
387 isotopic fractionation between NO and  $\text{NO}_2$  at various tropospheric atmospheric conditions.

388

#### 389 **4. Implications**

390 The daily variations of  $\Delta(\text{NO}_2\text{-NO}_x)$  values at two roadside  $\text{NO}_x$  monitoring sites were  
391 predicted to demonstrate the effects of  $\text{NO}_x$  concentrations to the NO- $\text{NO}_2$  isotopic fractionations.  
392 Hourly NO and  $\text{NO}_2$  concentrations were acquired from a roadside site at Anaheim, CA  
393 (<https://www.arb.ca.gov>) and an urban site at Evansville, IN (<http://idem.tx.sutron.com>) on July  
394 25, 2018. The hourly  $j(\text{NO}_2)$  values output from the TUV model (Madronich & Flocke, 1999) at  
395 these locations was used to calculate the daily variations of  $\Delta(\text{NO}_2\text{-NO}_x)$  values (Fig. 3A, B) by  
396 applying Eq. (8). Hourly  $\text{NO}_x$  concentrations were 12-51  $\text{nmol mol}^{-1}$  at Anaheim and 9-38  $\text{nmol}$   
397  $\text{mol}^{-1}$  at Evansville and the  $f(\text{NO}_2)$  values at both sites did not show significant daily variations  
398 ( $0.45\pm 0.07$  at Anaheim and  $0.65\pm 0.08$  at Evansville), likely because the  $\text{NO}_x$  concentrations were  
399 controlled by the high NO emissions from the road (Gao, 2007). The calculated  $\Delta(\text{NO}_2\text{-NO}_x)$

400 values using Eq. (8) showed significant diurnal variations. During the nighttime, the isotopic  
401 fractionations were solely controlled by the EIE, the predicted  $\Delta(\text{NO}_2\text{-NO}_x)$  values were  
402  $+14.5\pm 2.0$  ‰ and  $+8.7\pm 2.1$  ‰ at Anaheim and Evansville, respectively. During the daytime, the  
403 existence of LCIE lowered the predicted  $\Delta(\text{NO}_2\text{-NO}_x)$  values to  $+9.8\pm 1.7$  ‰ at Anaheim and  
404  $+3.1\pm 1.5$  ‰ at Evansville while the  $f(\text{NO}_2)$  values at both sites remained similar. The lowest  
405  $\Delta(\text{NO}_2\text{-NO}_x)$  values for both sites ( $+7.0$  ‰ and  $+1.7$  ‰) occurred around noon when the  $\text{NO}_x$   
406 photolysis was the most intense. In contrast, if one neglects the LCIE factor in the daytime, the  
407  $\Delta(\text{NO}_2\text{-NO}_x)$  values would be  $+12.9\pm 1.5$  ‰ and  $+10.0\pm 1.6$  ‰ respectively, an overestimation of  
408 3.1 ‰ and 6.9 ‰. These discrepancies suggested that the LCIE played an important role in the  
409  $\text{NO-NO}_2$  isotopic fractionations and neglecting it could bias the  $\text{NO}_x$  source apportionment using  
410  $\delta^{15}\text{N}$  of  $\text{NO}_2$  or nitrate.

411 The role of LCIE was more important in less polluted sites. The  $\Delta(\text{NO}_2\text{-NO}_x)$  values  
412 calculated for a suburban site near San Diego, CA, USA, again using the hourly  $\text{NO}_x$   
413 concentrations (<https://www.arb.ca.gov>, Fig. 3C) and  $j(\text{NO}_2)$  values calculated from the TUV  
414 model.  $\text{NO}_x$  concentrations at this site varied from 1 to 9  $\text{nmol mol}^{-1}$ . During the nighttime,  $\text{NO}_x$   
415 was in the form of  $\text{NO}_2$  ( $f(\text{NO}_2) = 1$ ) because  $\text{O}_3$  concentrations were higher than  $\text{NO}_x$ , thus the  
416  $\delta(\text{NO}_2)$  values should be identical to  $\delta(\text{NO}_x)$  ( $\Delta(\text{NO}_2\text{-NO}_x) = 0$ ). In the daytime a certain amount  
417 of  $\text{NO}$  was produced by direct  $\text{NO}$  emission and  $\text{NO}_2$  photolysis but the  $f(\text{NO}_2)$  was still high  
418 ( $0.73\pm 0.08$ ). Our calculation suggested the daytime  $\Delta(\text{NO}_2\text{-NO}_x)$  values should be only  $+1.3\pm 3.2$  ‰  
419 with a lowest value of  $-1.3$  ‰. These  $\Delta(\text{NO}_2\text{-NO}_x)$  values were similar to the observed and modeled  
420 summer daytime  $\delta(\text{NO}_2)$  values in West Lafayette, IN (Walters et al., 2018), which suggest the  
421 average daytime  $\Delta(\text{NO}_2\text{-NO}_x)$  values at  $\text{NO}_x = 3.9\pm 1.2$   $\text{nmol mol}^{-1}$  should range from  $+0.1$  ‰ to

422 +2.4 ‰. In this regime, we suggest the  $\Delta(\text{NO}_2\text{-NO}_x)$  values were generally small due to the  
423 significant contribution of LCIE and high  $f(\text{NO}_2)$ .

424 The LCIE should be the dominant factor controlling the NO-NO<sub>2</sub> isotopic fractionation at  
425 remote regions, resulting in a completely different diurnal pattern of  $\Delta(\text{NO}_2\text{-NO}_x)$  compared with  
426 the urban-suburban area. Direct hourly measurements of NO<sub>x</sub> at remote sites are rare, thus we used  
427 total NO<sub>x</sub> concentration of 50 pmol mol<sup>-1</sup>, daily O<sub>3</sub> concentration of 20 nmol mol<sup>-1</sup> at Summit,  
428 Greenland (Dibb et al., 2002; Hastings et al., 2004; Honrath et al., 1999; Yang et al., 2002), and  
429 assumed the conversion of NO to NO<sub>2</sub> was completely controlled by O<sub>3</sub> to calculate the NO/NO<sub>2</sub>  
430 ratios. Here the isotopes of NO<sub>x</sub> were almost exclusively controlled by the LCIE due to the high  
431 A values (>110). The  $\Delta(\text{NO}_2\text{-NO}_x)$  values displayed a clear diurnal pattern (Fig. 3D) with highest  
432 value of -0.3 ‰ in the “nighttime” (solar zenith angle >85 degree) and lowest value of -5.0 ‰ in  
433 the mid-day. This suggest that the isotopic fractionations between NO and NO<sub>2</sub> were almost  
434 completely controlled by LCIE at remote regions, when NO<sub>x</sub> concentrations were <0.1 nmol mol<sup>-1</sup>.  
435 However, since the isotopic fractionation factors of nitrate-formation reactions (NO<sub>2</sub>+OH,  
436 NO<sub>3</sub>+HC, N<sub>2</sub>O<sub>5</sub>+H<sub>2</sub>O) are still unknown, more studies are needed to fully explain the daily and  
437 seasonal variations of  $\delta(\text{NO}_3^-)$  at remote regions.

438 Nevertheless, our results have a few limitations. First, currently there are very few field  
439 observations that can be used to evaluate our model, therefore, future field observations that  
440 measure the  $\delta^{15}\text{N}$  values of ambient NO and NO<sub>2</sub> should be carried out to test our model. Second,  
441 more work, including theoretical and experimental studies, is needed to investigate the isotope  
442 fractionation factors occurring during the conversion from NO<sub>x</sub> to NO<sub>y</sub> and nitrate: in the NO<sub>y</sub>  
443 cycle, EIE (isotopic exchange between NO<sub>2</sub>, NO<sub>3</sub> and N<sub>2</sub>O<sub>5</sub>), KIE (formation of NO<sub>3</sub>, N<sub>2</sub>O<sub>5</sub> and  
444 nitrate) and PHIFE (photolysis of NO<sub>3</sub>, N<sub>2</sub>O<sub>5</sub>, HONO and sometimes nitrate) may also exist and

445 be relevant for the  $\delta^{15}\text{N}$  of  $\text{HNO}_3$  and HONO. In particular, the N isotope fractionation occurring  
446 during the  $\text{NO}_2 + \text{OH} \rightarrow \text{HNO}_3$  reaction needs investigation. Such studies could help us modeling  
447 the isotopic fractionation between  $\text{NO}_x$  emission and nitrate, and eventually enable us to analyze  
448 the  $\delta^{15}\text{N}$  value of  $\text{NO}_x$  emission by measuring the  $\delta^{15}\text{N}$  values of nitrate aerosols and nitrate in wet  
449 depositions. Third, our discussion only focuses on the reactive nitrogen chemistry in the  
450 troposphere, however, the nitrogen chemistry in the stratosphere is drastically different from the  
451 tropospheric chemistry, thus future studies are also needed to investigate the isotopic fractionations  
452 in the stratospheric nitrogen chemistry. Last, the temperature dependence of both EIE and LCIE  
453 needs to be carefully investigated, because of the wide range of temperature in both troposphere  
454 and stratosphere. Changes in temperature could alter the isotopic fractionation factors of both EIE  
455 and LCIE, as well as contribute to the seasonality of isotopic fractionations between  $\text{NO}_x$  and  $\text{NO}_y$   
456 molecules.

Deleted: because of the wide

Deleted: , and the

Deleted: dependence

Deleted: also

457

## 458 5. Conclusions

459 The effect of  $\text{NO}_x$  photochemistry on the nitrogen isotopic fractionations between NO and  
460  $\text{NO}_2$  was investigated. We first measured the isotopic fractionations between NO and  $\text{NO}_2$  and  
461 provided mathematical solutions to assess the impact of  $\text{NO}_x$  level and  $\text{NO}_2$  photolysis rate ( $j(\text{NO}_2)$ )  
462 to the relative importance of EIE and LCIE. The EIE and LCIE isotope fractionation factors, at  
463 room temperature, were determined to be  $1.0275 \pm 0.0012$  and  $0.990 \pm 0.005$ , respectively. These  
464 calculations and measurements can be used to determine the steady state  $\Delta(\text{NO}_2\text{-NO})$  and  $\Delta(\text{NO}_2\text{-}$   
465  $\text{NO}_x)$  values at room temperature. Subsequently we applied our equations to polluted, clean and  
466 remote sites to model the daily variations of  $\Delta(\text{NO}_2\text{-NO}_x)$  values. We found that the  $\Delta(\text{NO}_2\text{-NO}_x)$   
467 values could vary from over +20 ‰ to less than -5 ‰ depending on the environment: in general,

472 the role of LCIE becoming more important at low NO<sub>x</sub> concentrations, which tend to decrease the  
473  $\Delta(\text{NO}_2\text{-NO}_x)$  values. Our work provided a mathematical approach to quantify the nitrogen isotopic  
474 fractionations between NO and NO<sub>2</sub> that can be applied to many tropospheric environments, which  
475 could help interpret the measured  $\delta^{15}\text{N}$  values of NO<sub>2</sub> and nitrate in field observation studies.

476

#### 477 **Acknowledgement**

478 We thank NCAR's Advanced Study Program granted to Jianghanyang Li. The National  
479 Center for Atmospheric Research is operated by the University Corporation for Atmospheric  
480 Research, under the sponsorship of the National Science Foundation. We also thank funding  
481 support from Purdue Climate Change Research Center and A. H. Ismail Interdisciplinary Program  
482 Doctoral Research Travel Award granted by Purdue University.

#### 483 **Data Availability**

484 Data acquired from this study was deposited at Open Sciences Framework (Li, 2019,  
485 DOI 10.17605/OSF.IO/JW8HU).

#### 486 **Author contribution**

487 J. Li and G. Michalski designed the experiments, X. Zhang and J. Li conducted the  
488 experiments. X. Zhang, G. Michalski, J. Orlando and G. Tyndall helped J. Li in interpreting the  
489 results. The manuscript was written by J. Li and all the authors have contributed during the revision  
490 of this manuscript.

#### 491 **Competing interest**

492 The authors declare no competing interest.

493

#### 494 **References:**

495



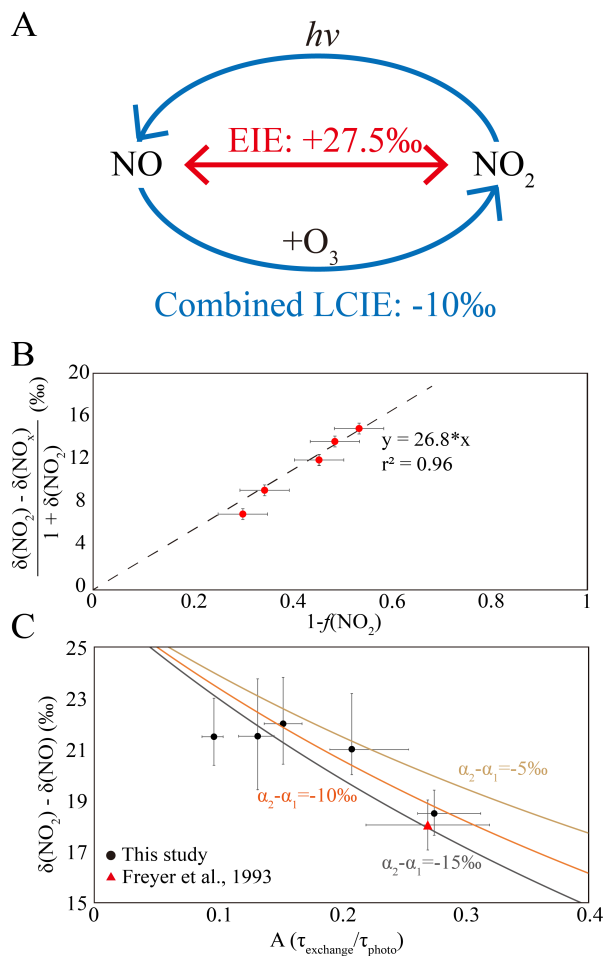
496 Atkinson, R., Baulch, D. L., Cox, R. A., Crowley, J. N., Hampson, R. F., Hynes, R. G., et al. (2004).  
497 Evaluated kinetic and photochemical data for atmospheric chemistry: Volume I-gas phase  
498 reactions of O<sub>x</sub>, HO<sub>x</sub>, NO<sub>x</sub> and SO<sub>x</sub> species. *Atmospheric Chemistry and Physics*, 4(6), 1461–1738.  
499  
500 Barney, W. S., & Finlayson-Pitts, B. J. (2000). Enhancement of N<sub>2</sub>O<sub>4</sub> on porous glass at room  
501 temperature: A key intermediate in the heterogeneous hydrolysis of NO<sub>2</sub>? *The Journal of Physical*  
502 *Chemistry A*, 104(2), 171–175.  
503  
504 Begun, G. M., & Fletcher, W. H. (1960). Partition function ratios for molecules containing  
505 nitrogen isotopes. *The Journal of Chemical Physics*, 33(4), 1083–1085.  
506  
507 Begun, G. M., & Melton, C. E. (1956). Nitrogen isotopic fractionation between NO and NO<sub>2</sub> and  
508 mass discrimination in mass analysis of NO<sub>2</sub>. *The Journal of Chemical Physics*, 25(6), 1292–1293.  
509  
510 Beine, H. J., Honrath, R. E., Dominé, F., Simpson, W. R., & Fuentes, J. D. (2002). NO<sub>x</sub> during  
511 background and ozone depletion periods at Alert: Fluxes above the snow surface. *Journal of*  
512 *Geophysical Research: Atmospheres*, 107(D21), ACH-7.  
513  
514 Bigeleisen, J., & Mayer, M. G. (1947). Calculation of equilibrium constants for isotopic exchange  
515 reactions. *The Journal of Chemical Physics*, 15(5), 261-267.  
516  
517 Bigeleisen, J., & Wolfsberg, M. (1957). Theoretical and experimental aspects of isotope effects in  
518 chemical kinetics. *Advances in Chemical Physics*, 15–76.  
519  
520 Casciotti, K. L., & McIlvin, M. R. (2007). Isotopic analyses of nitrate and nitrite from reference  
521 mixtures and application to Eastern Tropical North Pacific waters. *Marine Chemistry*, 107(2), 184–  
522 201.  
523  
524 Chang, Y., Zhang, Y., Tian, C., Zhang, S., Ma, X., Cao, F., et al. (2018). Nitrogen isotope  
525 fractionation during gas-to-particle conversion of NO<sub>x</sub> to NO<sub>3</sub><sup>-</sup> in the atmosphere—implications for  
526 isotope-based NO<sub>x</sub> source apportionment. *Atmospheric Chemistry and Physics*, 18(16), 11647–  
527 11661.  
528  
529 Clapp, L. J., & Jenkin, M. E. (2001). Analysis of the relationship between ambient levels of O<sub>3</sub>,  
530 NO<sub>2</sub> and NO as a function of NO<sub>x</sub> in the UK. *Atmospheric Environment*, 35(36), 6391–6405.  
531  
532 Custard, K. D., Thompson, C. R., Pratt, K. A., Shepson, P. B., Liao, J., Huey, L. G., et al. (2015).  
533 The NO<sub>x</sub> dependence of bromine chemistry in the Arctic atmospheric boundary layer. *Atmospheric*  
534 *Chemistry and Physics*, 15(18), 10799–10809.  
535  
536 Dibb, J. E., Arsenault, M., Peterson, M. C., & Honrath, R. E. (2002). Fast nitrogen oxide  
537 photochemistry in Summit, Greenland snow. *Atmospheric Environment*, 36(15–16), 2501–2511.  
538  
539 Do Remus, R. H., Mehrotra, Y., Lanford, W. A., & Burman, C. (1983). Reaction of water with  
540 glass: influence of a transformed surface layer. *Journal of Materials Science*, 18(2), 612–622.  
541

542 Elliott, E. M., Kendall, C., Boyer, E. W., Burns, D. A., Lear, G. G., Golden, H. E., et al. (2009).  
543 Dual nitrate isotopes in dry deposition: Utility for partitioning NO<sub>x</sub> source contributions to  
544 landscape nitrogen deposition. *Journal of Geophysical Research: Biogeosciences*, 114(G4),  
545 G04020. <https://doi.org/10.1029/2008JG000889>  
546  
547 Felix, J. D., & Elliott, E. M. (2014). Isotopic composition of passively collected nitrogen dioxide  
548 emissions: Vehicle, soil and livestock source signatures. *Atmospheric Environment*, 92, 359–366.  
549  
550 Felix, J. D., Elliott, E. M., & Shaw, S. L. (2012). Nitrogen isotopic composition of coal-fired power  
551 plant NO<sub>x</sub>: influence of emission controls and implications for global emission inventories.  
552 *Environmental Science & Technology*, 46(6), 3528–3535.  
553  
554 Frey, M. M., Savarino, J., Morin, S., Erbland, J., & Martins, J. M. F. (2009). Photolysis imprint in  
555 the nitrate stable isotope signal in snow and atmosphere of East Antarctica and implications for  
556 reactive nitrogen cycling. *Atmos. Chem. Phys*, 9, 8681–8696.  
557  
558 Freyer, H. D. (1991). Seasonal variation of <sup>15</sup>N/<sup>14</sup>N ratios in atmospheric nitrate species. *Tellus B*,  
559 43(1), 30–44. <https://doi.org/10.1034/j.1600-0889.1991.00003.x>  
560  
561 Freyer, H. D., Kley, D., Volz-Thomas, A., & Kobel, K. (1993). On the interaction of isotopic  
562 exchange processes with photochemical reactions in atmospheric oxides of nitrogen. *Journal of*  
563 *Geophysical Research: Atmospheres*, 98(D8), 14791–14796.  
564  
565 Gao, H. O. (2007). Day of week effects on diurnal ozone/NO<sub>x</sub> cycles and transportation emissions  
566 in Southern California. *Transportation Research Part D: Transport and Environment*, 12(4), 292–  
567 305.  
568  
569 Gobel, A. R., Altieri, K. E., Peters, A. J., Hastings, M. G., & Sigman, D. M. (2013). Insights into  
570 anthropogenic nitrogen deposition to the North Atlantic investigated using the isotopic  
571 composition of aerosol and rainwater nitrate. *Geophysical Research Letters*, 40(22), 5977–5982.  
572 <https://doi.org/10.1002/2013GL058167>  
573  
574 Hastings, M G, Jarvis, J. C., & Steig, E. J. (2009). Anthropogenic impacts on nitrogen isotopes of  
575 ice-core nitrate. *Science*, 324(5932), 1288.  
576  
577 Hastings, M G, Steig, E. J., & Sigman, D. M. (2004). Seasonal variations in N and O isotopes of  
578 nitrate in snow at Summit, Greenland: Implications for the study of nitrate in snow and ice cores.  
579 *Journal of Geophysical Research: Atmospheres*, 109(D20).  
580  
581 Hoefs, J. (2009). *Stable isotope geochemistry* (Vol. 285). Springer.  
582  
583 Honrath, R. E., Peterson, M. C., Guo, S., Dibb, J. E., Shepson, P. B., & Campbell, B. (1999).  
584 Evidence of NO<sub>x</sub> production within or upon ice particles in the Greenland snowpack. *Geophysical*  
585 *Research Letters*, 26(6), 695–698.  
586

587 Jarvis, J. C., Steig, E. J., Hastings, M. G., & Kunasek, S. A. (2008). Influence of local  
588 photochemistry on isotopes of nitrate in Greenland snow. *Geophysical Research Letters*, 35(21).  
589 Kendall, C., Elliott, E. M., & Wankel, S. D. (2007). Tracing anthropogenic inputs of nitrogen to  
590 ecosystems. *Stable Isotopes in Ecology and Environmental Science*, 2, 375–449.  
591  
592 Kimbrough, S., Owen, R. C., Snyder, M., & Richmond-Bryant, J. (2017). NO to NO<sub>2</sub> conversion  
593 rate analysis and implications for dispersion model chemistry methods using Las Vegas, Nevada  
594 near-road field measurements. *Atmospheric Environment*, 165, 23–34.  
595  
596 King, Martin D., Carlos E. Canosa-Mas, and Richard P. Wayne. "Gas-phase reactions between  
597 RO<sub>2</sub> and NO, HO<sub>2</sub> or CH<sub>3</sub>O<sub>2</sub>: correlations between rate constants and the SOMO energy of the  
598 peroxy (RO<sub>2</sub>) radical." *Atmospheric Environment* 35.12 (2001): 2081-2088.  
599  
600 Knote, Christoph, et al. "Influence of the choice of gas-phase mechanism on predictions of key  
601 gaseous pollutants during the AQMEII phase-2 intercomparison." *Atmospheric Environment* 115  
602 (2015): 553-568.  
603  
604 Li, J. (2019). Quantifying the nitrogen equilibrium and photochemistry-induced kinetic isotopic  
605 effects between NO and NO<sub>2</sub>. Retrieved from [osf.io/jw8hu](https://osf.io/jw8hu)  
606  
607 Madronich, S., & Flocke, S. (1999). The role of solar radiation in atmospheric chemistry. In  
608 *Environmental photochemistry* (pp. 1–26). Springer.  
609  
610 Mazzeo, N. A., Venegas, L. E., & Choren, H. (2005). Analysis of NO, NO<sub>2</sub>, O<sub>3</sub> and NO<sub>x</sub>  
611 concentrations measured at a green area of Buenos Aires City during wintertime. *Atmospheric*  
612 *Environment*, 39(17), 3055–3068.  
613  
614 McIlvin, M. R., & Altabet, M. A. (2005). Chemical conversion of nitrate and nitrite to nitrous  
615 oxide for nitrogen and oxygen isotopic analysis in freshwater and seawater. *Analytical Chemistry*,  
616 77(17), 5589–5595.  
617  
618 Michalski, G., Jost, R., Sugny, D., Joyeux, M., & Thiemens, M. (2004). Dissociation energies of  
619 six NO<sub>2</sub> isotopologues by laser induced fluorescence spectroscopy and zero-point energy of some  
620 triatomic molecules. *The Journal of Chemical Physics*, 121(15), 7153–7161.  
621  
622 Michalski, G., Bockheim, J. G., Kendall, C., & Thiemens, M. (2005). Isotopic composition of  
623 Antarctic Dry Valley nitrate: Implications for NO<sub>x</sub> sources and cycling in Antarctica. *Geophysical*  
624 *Research Letters*, 32(13).  
625  
626 Miller, C. E., & Yung, Y. L. (2000). Photo-induced isotopic fractionation. *Journal of Geophysical*  
627 *Research: Atmospheres*, 105(D23), 29039–29051.  
628  
629 Monse, E. U., Spindel, W., & Stern, M. J. (1969). Analysis of isotope-effect calculations illustrated  
630 with exchange equilibria among oxynitrogen compounds. Rutgers-The State Univ., Newark, NJ.  
631

632 Morin, S., Savarino, J., Frey, M. M., Domine, F., Jacobi, H.-W., Kaleschke, L., & Martins, J. M.  
633 F. (2009). Comprehensive isotopic composition of atmospheric nitrate in the Atlantic Ocean  
634 boundary layer from 65°S to 79°N. *J. Geophys. Res.*, 114. <https://doi.org/10.1029/2008JD010696>  
635  
636 Park, Y.-M., Park, K.-S., Kim, H., Yu, S.-M., Noh, S., Kim, M.-S., et al. (2018). Characterizing  
637 isotopic compositions of TC-C, NO<sub>3</sub><sup>-</sup>-N, and NH<sub>4</sub><sup>+</sup>-N in PM<sub>2.5</sub> in South Korea: Impact of China's  
638 winter heating. <https://doi.org/10.1016/j.envpol.2017.10.072>  
639  
640 Saliba, N. A., Yang, H., & Finlayson-Pitts, B. J. (2001). Reaction of gaseous nitric oxide with  
641 nitric acid on silica surfaces in the presence of water at room temperature. *The Journal of Physical*  
642 *Chemistry A*, 105(45), 10339–10346.  
643  
644 Savarino, J., Morin, S., Erbland, J., Grannec, F., Patey, M. D., Vicars, W., et al. (2013). Isotopic  
645 composition of atmospheric nitrate in a tropical marine boundary layer. *Proceedings of the*  
646 *National Academy of Sciences*, 110(44), 17668–17673. <https://doi.org/10.1073/pnas.1216639110>  
647  
648 Sharma, H. D., Jervis, R. E., & Wong, K. Y. (1970). Isotopic exchange reactions in nitrogen oxides.  
649 *The Journal of Physical Chemistry*, 74(4), 923–933.  
650  
651 Takei, T., Yamazaki, A., Watanabe, T., & Chikazawa, M. (1997). Water adsorption properties on  
652 porous silica glass surface modified by trimethylsilyl groups. *Journal of Colloid and Interface*  
653 *Science*, 188(2), 409–414.  
654  
655 Urey, H. C. (1947). The thermodynamic properties of isotopic substances. *Journal of the Chemical*  
656 *Society (Resumed)*, 562-581.  
657  
658 Vicars, W. C., Morin, S., Savarino, J., Wagner, N. L., Erbland, J., Vince, E., et al. (2013). Spatial  
659 and diurnal variability in reactive nitrogen oxide chemistry as reflected in the isotopic composition  
660 of atmospheric nitrate: Results from the CalNex 2010 field study. *Journal of Geophysical Research:*  
661 *Atmospheres*, 118(18), 10–567.  
662  
663 Walters, W. W., & Michalski, G. (2015). Theoretical calculation of nitrogen isotope equilibrium  
664 exchange fractionation factors for various NO<sub>y</sub> molecules. *Geochimica et Cosmochimica Acta*,  
665 164, 284–297.  
666  
667 Walters, W. W., Goodwin, S. R., & Michalski, G. (2015). Nitrogen stable isotope composition  
668 (δ<sup>15</sup>N) of vehicle-emitted NO<sub>x</sub>. *Environmental Science & Technology*, 49(4), 2278–2285.  
669  
670 Walters, W. W., & Michalski, G. (2016). Ab initio study of nitrogen and position-specific oxygen  
671 kinetic isotope effects in the NO+O<sub>3</sub> reaction. *The Journal of chemical physics*, 145(22), 224311.  
672  
673 Walters, W. W., Simonini, D. S., & Michalski, G. (2016). Nitrogen isotope exchange between NO  
674 and NO<sub>2</sub> and its implications for δ<sup>15</sup>N variations in tropospheric NO<sub>x</sub> and atmospheric nitrate.  
675 *Geophysical Research Letters*, 43(1), 440–448.  
676

- 677 Walters, W. W., Fang, H., & Michalski, G. (2018). Summertime diurnal variations in the isotopic  
678 composition of atmospheric nitrogen dioxide at a small midwestern United States city.  
679 *Atmospheric Environment*, 179, 1–11.  
680
- 681 Williams, E. L., & Grosjean, D. (1990). Removal of atmospheric oxidants with annular denuders.  
682 *Environmental Science & Technology*, 24(6), 811–814.  
683
- 684 Yang, J., Honrath, R. E., Peterson, M. C., Dibb, J. E., Sumner, A. L., Shepson, P. B., et al. (2002).  
685 Impacts of snowpack emissions on deduced levels of OH and peroxy radicals at Summit,  
686 Greenland. *Atmospheric Environment*, 36(15–16), 2523–2534.  
687
- 688 Zhang, X., Ortega, J., Huang, Y., Shertz, S., Tyndall, G. S., & Orlando, J. J. (2018). A steady-state  
689 continuous flow chamber for the study of daytime and nighttime chemistry under atmospherically  
690 relevant NO levels. *Atmospheric Measurement Techniques*, 11(5), 2537–2551.  
691
- 692 Zong, Z., Wang, X., Tian, C., Chen, Y., Fang, Y., Zhang, F., et al. (2017). First assessment of NO<sub>x</sub>  
693 sources at a regional background site in North China using isotopic analysis linked with modeling.  
694 *Environmental Science & Technology*, 51(11), 5923–5931.



695  
696  
697  
698  
699  
700  
701  
702  
703

**Fig. 1** **A**, a sketch of the isotopic fractionation processes between NO and NO<sub>2</sub>, both fractionation factors are determined in this work. **B**, Results from five dark experiments yielded a line with  $\epsilon(\text{NO}_2\text{-NO})/(1+\epsilon(\text{NO}_2\text{-NO}))$  value of 26.8 ‰ and  $\epsilon(\text{NO}_2\text{-NO})$  value of 27.5 ‰; **C**, Results from five UV irradiation experiments (black points) and a previous field study (red triangle). The three lines represent different  $(\alpha_2-\alpha_1)$  values: the  $(\alpha_2-\alpha_1)=-10\text{‰}$  line showed the lowest RMSE to our experimental data as well as the previous field observation. The error bars in panels B and C represented the combined uncertainties of NO<sub>x</sub> concentration measurements and isotopic analysis.

**Deleted:**  $\delta^{15}\text{N}$  of NO<sub>2</sub> collected in dark and UV irradiation experiments.

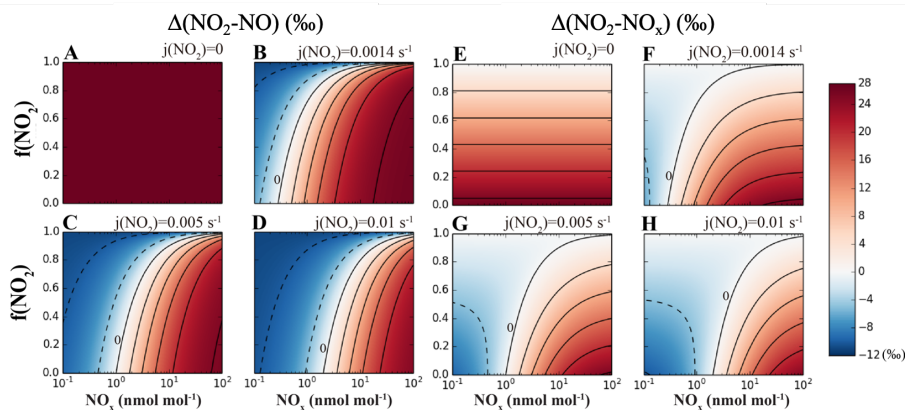
**Deleted:** A

**Deleted:** B

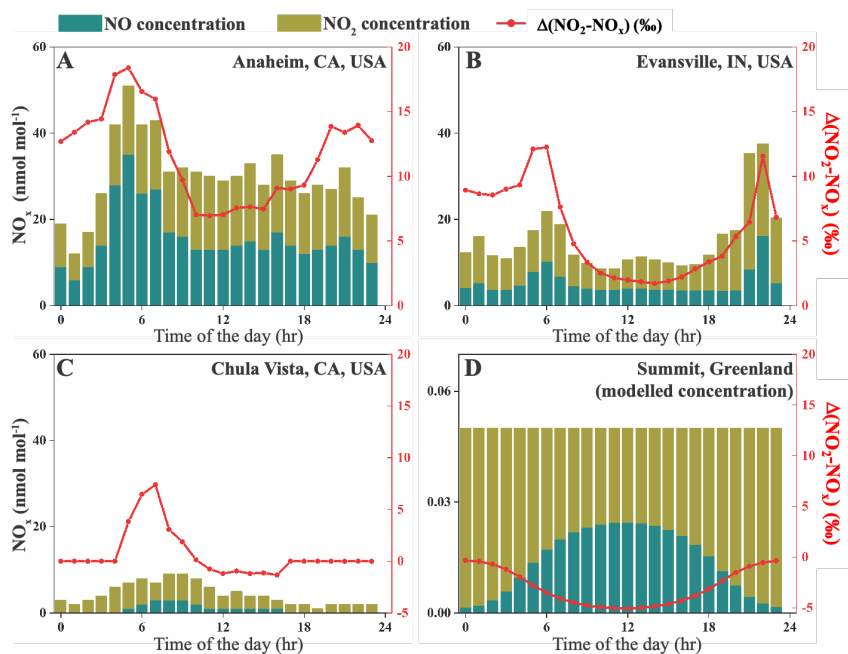
**Deleted:** best fit

**Deleted:** ; C. a sketch of the isotopic fractionation processes between NO and NO<sub>2</sub>

**Formatted:** Subscript



711  
 712 **Fig. 2** Calculating isotopic fractionation values between NO-NO<sub>2</sub> ( $\Delta(\text{NO}_2\text{-NO})$ , **A-D**) and NO<sub>x</sub>-  
 713 NO<sub>2</sub> ( $\Delta(\text{NO}_2\text{-NO}_x)$ , **E-H**) at various  $j(\text{NO}_2)$ , NO<sub>x</sub> level and  $f(\text{NO}_2)$  using Eq. (7) and (8). Each  
 714 panel represents a fixed  $j(\text{NO}_2)$  value (showing on the upper right side of each panel), and the  
 715 fractionation values are shown by color. Lines are contours with the same fractionation values, at  
 716 an interval of 5‰, the contour line representing 0‰ was marked on each panel except for A and  
 717 E.



718  
719  
720  
721  
722

**Fig. 3** NO<sub>x</sub> concentrations and calculated  $\Delta(\text{NO}_2-\text{NO}_x)$  values at four sites. Stacked bars show the NO and NO<sub>2</sub> concentrations extracted from monitoring sites (A-C) or calculated using 0-D box model (D); the red lines are  $\Delta(\text{NO}_2-\text{NO}_x)$  values at each site. *Note that the NO<sub>x</sub> concentration (left-y) axis on panel D is different from the rest.*

Formatted: Subscript